ACS APPLIED ENERGY MATERIALS

www.acsaem.org Article

Stability of Solid-Electrolyte Interphase (SEI) on the Lithium Metal Surface in Lithium Metal Batteries (LMBs)

Ajaykrishna Ramasubramanian,* Vitaliy Yurkiv, Tara Foroozan, Marco Ragone, Reza Shahbazian-Yassar, and Farzad Mashayek

Cite This: https://dx.doi.org/10.1021/acsaem.0c01605 Read Online

ACCESS | Metrics & More | Article Recommendations | Supporting Information

ABSTRACT: The structural character and mechanical stability of solid-electrolyte interphase (SEI) play a critical role in the formation of dendrites in lithium metal batteries (LMBs). However, due to the complex structures of SEI, the mechanisms by which dendrites nucleate at the interface of Li metal and SEI layer are not well understood. In this work, we employed first-principles calculations using density functional theory (DFT) to study the stability of the innermost layer of the grain-structured SEI on the Li metal surface. The grain structures of LiF/LiF, Li_2O/Li_2O, and LiF/Li_2O and their interaction with the Li surface are considered. The stability of different SEI grain structures is analyzed based on the overpotential due to Li addition. Also, the excess energies required for SEI components to crack along their grain boundary (GB) defects are investigated. The initial observation of these structures suggests that there is a significant rearrangement in the interfacial layers (first few layers) of Li. The system reaches a metastable state when more Li is added to the GB and/or to the triple-phase boundary (TPB) between the GB and Li surface. The energetics from the DFT calculations vary significantly depending upon the grain structures, with LiF/LiF grain structures being the most stable and LiF/Li_2O being the least stable. The calculated energies, with and without vacancies, at the TPB region of Li/SEI interfaces, show that the interface between Li_2O/Li_2O on Li is the least favorable energetically and more susceptible to stress accumulation and cracking followed by LiF/Li_2O on Li and LiF/LiF on Li, respectively.

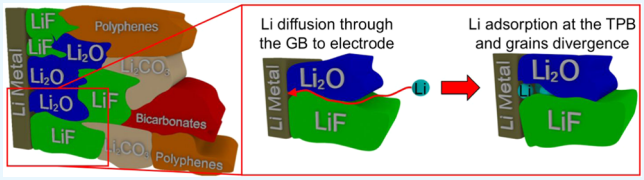

KEYWORDS: *lithium metal batteries (LMBs), solid-electrolyte interphase (SEI), density functional theory (DFT), grain boundary (GB), triple-phase boundary (TPB)*

1. INTRODUCTION

In recent years, lithium metal-based batteries (LMBs) are regarded as the most promising alternatives to lithium-ion batteries (LIBs).[1,2] Lithium (Li) metal anode has been an attractive anode material because of its high theoretical capacity (3860 mA/(h g)), low material density (0.59 g cm^{-3}), and low electrochemical potential (−3.04 V).[3,4] However, their commercial application is severely restricted due to the dendritic growth of Li and resulting low Coulomb efficiency during cell cycling.[4−6] Among these problems, the growth of dendrites is regarded as the most challenging. The dendritic growth of Li, if left uncontrolled, can penetrate through the separator and short the cell leading to thermal runaway, fires, and catastrophic failures in LMBs.[7−9] Thus, dendrite prevention is a significant factor significant in addressing battery reliability and safety concerns. To control the growth direction of Li dendrites, the determination of Li nucleation sites during deposition is critically important.

The most characteristic feature of electrodeposition in Li metal anodes is the formation of solid-electrolyte interphase (SEI). The SEI forms due to electrolyte reduction on the Li surface. This layer was first identified and introduced by Peled et al.[10] in 1979 as SEI and further improved and clarified in their later work by suggesting the existence of anisotropic grained structure.[11−13] The SEI layer acts as a transport medium for the Li ion between the electrolyte to the anode surface and also prevents more unfavorable reactions that lead to further depletion of electrolyte and the Li metal surface.[14,15] However, as shown in our previous work,[16] the defects in the SEI layer allow for a significant anisotropic diffusion of Li toward the anode surface, leading to random electrodeposition and dendritic formation.

Despite the best efforts from experimentalists, very few studies have been dedicated to addressing the influence of GB in SEI using in situ transition electron microscopy.[17,18] This is because imaging of lithium dendrites is immensely challenging during the normal operation of a cell until the dendrites grow to a size of 100 nm and enter a rapid growth phase. Also, imaging the atomic-scale inhomogeneities on the electrode

Received: July 8, 2020
Accepted: October 26, 2020

surface, which act as the nucleation spots for the dendrites, is even more challenging due to its length scales, elemental composition, and high reactivity of the components at the interphase. Therefore, a comprehensive modeling effort is required to understand and address this issue with LMBs as addressed in some of the previous literature.[19]

In prior literature, some researchers have focused on capturing the evolution of lithium dendrites numerically. Gibbs et al.[20] developed a new tomographic reconstruction algorithm to simulate the morphology changes in three-dimensional (3D) metallic dendrites. Qin et al.[21] used density functional theory (DFT) to analyze the electron transfer between lithium (100) and lithium cations near the surface. They also summarized that the heterogeneous nucleation and growth of lithium is promoted by the strong heterogeneous electron distribution. Aryanfar et al.[22] used Monte Carlo method to simulate the Li growth and showed that the electric field at the sharp tip of a dendrite accelerates the dendrite growth. Yoon et al.[23] used COMSOL to simulate the Li deposition and stripping and showed that the high electric field at the tip of dendrite allows for faster growth of dendrites.[23] Yurkiv et al.,[6] Yan et al.,[7] and Hong et al.[24] studied the evolution and growth of dendrites and the effect of SEI on its evolution through phase-field simulations. Liu et al.[25] presented a comprehensive mathematical model that concurrently couples the Li dendrite growth and the effect of SEI through cracking of the SEI layer and SEI regrowth. These theoretical models have given far deeper physical insights on the Li dendrite evolution and growth process. However, all of these theoretical studies lack in addressing the initial nucleation of Li dendrites and the role of heterogenous SEI on dendritic nucleation and growth.

The prediction of the nucleation site of Li dendrite plays a significant role in determining the growing direction of dendritic branches during the electrodeposition process. Various viewpoints about the location and mechanism of nucleation of these dendrites have been proposed in the literature. This includes the surface nucleation and diffusion model,[26] heterogeneous nucleation model,[27] space-charge model,[28] and SEI-induced nucleation model.[29] However, most of these studies on dendrite formation in LMBs have focused on homogeneous SEI films. The most popular modeling strategy adopts a model similar to the electroplating of metal in water. The dendrites, in this case, arise only due to the local changes in electric fields because of surface roughness effects. While these viewpoints provide some useful strategies to suppress dendrites, they do not take into account the localized occurrences of lithium nucleation on the SEI film. In fact, the work of Peled et al.,[12] Christensen et al.,[30] and recently Leung et al.[31] and Yurkiv et al.[32] are the only studies supporting the idea of the existence of grain structures in SEI. However, none of these works focus on the mechanical and electronic stability of these heterogenous grained SEI components on the Li surface and their role in the nucleation of dendrites. The studies performed in Yurkiv et al.[32] are very similar to the present work but analyze Zn electrodeposition in Zinc aqueous batteries.

In our previous work,[16] we have identified the critical pathways of Li diffusion through the inorganic SEI grain structure and discussed in great detail its effects on anisotropic Li deposition and dendritic nucleation. Thus, in this work, as a natural extension, we analyze the stability of such SEI grain structures on the Li surface. This study follows the hypothesis that the nanoscale defects at the solid−solid interphases between the inner inorganic part of SEI and the Li metal surface are the primary sites where the SEI starts to crack in LMBs. While the focus of the current study is on the SEI in liquid electrolyte-based LMBs, the concepts are drawn from all solid batteries and from electronic materials, where dendritic growth is observed inside the pores and defects of the solid-electrolyte material.[33] Although Li_2CO_3 has been studied extensively as one of the components of the inorganic SEI layer,[34,35] there are numerous works in recent years that describe Li_2CO_3 as not a stable SEI component.[36−40] Other than the stability of Li_2CO_3 on the Li surface, as shown by Leung et al.,[31] several other reasons could contribute to its absence in the SEI. This includes aging of electrodes,[41,42] electrolyte type and its quality,[39] and hermetic-seals[36] on the lithium-ion cells. Therefore, we believe more experimental measurements are required to prove the presence of stable Li_2CO_3 in the innermost layer of the SEI, which falls beyond the scope of this work.

As mentioned in the previous paragraphs, the focus of the current work is on the GB interface of the inorganic SEI with the Li metal surface, to understand and evaluate the stability of such grained structures on the Li surface, their ability to accommodate Li atoms, and the excess energy of formation of the interface. Figure 1 provides a schematic on the focus of the current work by showing a grain-structured SEI with exaggerated inorganic and organic layers (LiF, Li_2O, and Li_2CO_3 being major inorganic components), followed by the addition of Li in the grain structure and the formation of cracks and dendritic growth. This work concentrates specifically on studying the stability of the GB structures of LiF/LiF, Li_2O/Li_2O, and LiF/Li_2O on the Li surface and their triple-phase boundaries (TPB), as they are the most prevalent inorganic components that naturally occur near the Li surface due to electrolyte decomposition.[16]

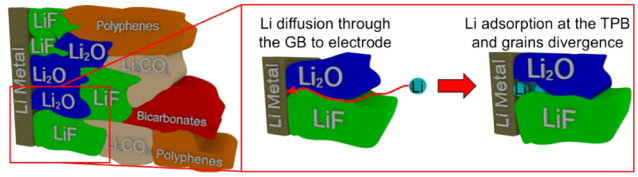

Figure 1. Schematic representation of the hypothesis in the present work. The left picture depicts an inner inorganic layer of SEI illustrating its grain structure and then the successive addition Li leading to the formation of cracks in the SEI grain structure.

Section 2 provides the details of the DFT framework, which is used in the current work to capture the stability and energetics of SEI components on the Li metal surface. In Section 3, the results showing stability characteristics and the energetics for different triple-phase boundaries (TPB) are presented. The stabilities are compared both quantitatively and qualitatively, and the excess energies of formation of the TPBs in different configurations are reported, which provides a good understanding of the nucleation sites of the dendrites. In Section 4, the findings and conclusions from the different comparisons are briefly summarized.

2. METHODOLOGY

The DFT calculations in the current work are performed using the Vienna Ab initio Simulation Package (VASP) code.[43] The

https://dx.doi.org/10.1021/acsaem.0c01605
ACS Appl. Energy Mater. XXXX, XXX, XXX−XXX

basis sets are defined by plane-wave basis sets, and a projector augmented wave (PAW)[44] pseudopotential in the framework of Perdew−Burke−Ernzerhof sol (PBEsol)[45] generalized gradient approximation (GGA)[46] is used for obtaining the ground-state energies.

Since the formation of the SEI film is kinetically driven, with many thermodynamically metastable components, modeling such a system with a proper account of the kinetic constraints is very complicated to construct systematically. The explanation of the formation of GB structures of SEI has already been discussed in detail in our previous work.[16] After generating the GB system of the SEI components, these are then placed on the most stable Li surfaces ((001) and (011) surface),[47] and the resulting interface structures are optimized. The Li facets are chosen and the Li metal slab is strained in such a way that it gives the best lattice matching with the SEI grain structure and also has the least strain at the interphase. The lattice mismatch between the Li slab and the SEI GB is between 2 and 4%, and it depends on the lattice structure of the SEI GB. The *z*-direction in all of the analyzed structures is kept perpendicular to the Li surface.

The optimized bulk lattice of Li is first calculated. Then, the slab method is used to calculate the most stable surfaces using the surface energies of Li, cleaved with various surface orientations. The *k*-point samplings are set appropriately for each surface structure optimization, with one *k*-point in the direction normal to the vacuum region. An equal number of in-plane *k*-points are defined for the surface structures as in the bulk calculations. These surfaces are then interfaced with the grained structures of SEI in such a way that the interphase is perpendicular to the GB in SEI. Additionally, to ensure that the thickness of the slab is chosen appropriately to represent the macroscopic properties of the crystal, the interphase energy is calculated for multiple different slab thicknesses. Nominal slab thickness is chosen for each system such that the change in interphase energy is less than 2% for a 5% increase in slab thickness. The simulation cell stoichiometries and *k*-point sampling are as shown in Table 1. Other calculations involve small variations on the cells listed in Table 1, such as the addition of the Li atom in the vacant TPB and GB regions. In all calculations, a dipole moment correction is applied and a spin polarization is applied if the supercell contains odd number of atoms.

Table 1. Summary of all of the GB Structures and Their Stoichiometry

chemical system	supercell stoichiometry	*k*-points
LiF/LiF ($\sum$5 GB) on Li	$Li_{184}F_{112}$	5 × 3 × 1
Li_2O/Li_2O ($\sum$3 GB) on Li	$Li_{192}O_{60}$	3 × 4 × 1
LiF/Li_2O GB on Li	$Li_{192}F_{48}O_{36}$	3 × 3 × 1

We would like to note that the scope of this work is not to capture the charge-transfer reaction as the time scale of the charge-transfer reaction falls well beyond the scope of atomistic-scale simulations in this work. Our simulation cell consists of an overall charge neutral interface structure of Li metal and SEI grain structure (i.e., 0.0 V vs Li^+/Li). In all of the cases that are simulated, the voltages in the interfacial simulation cell are determined by the lithium content and energetics. This assumption of overall charge neutrality simplifies the problem to a large extent and some effects of simulation cells constructed at different applied overpotential conditions as listed in Leung et al.[48,49] are not captured in this work. A 400 eV plane-wave energy cutoff is imposed. A maximum change in the total energy of less than 0.1 eV is observed across the different GB structures on increasing the cutoff energy to 450 eV. The force convergence criterion is set to 1 meV/Å.

3. RESULTS AND DISCUSSION

3.1. Stability of SEI GB on the Li Surface. As explained in the previous section, the GB structures of LiF/LiF, Li_2O/Li_2O, and LiF/Li_2O, as shown and discussed in our previous work,[16] are created. Then, the Li slabs with 001 and 110 surface orientations are created to identify the most stable surface for the GB interphase. The interphases are designed in such a way that the SEI GB is interfaced perpendicular to the Li slab, which renders only two possible orientations for the interphase. It was identified that the (001) surface of Li matches well with LiF/LiF, and LiF/Li_2O GB and the (110) surface of Li matches well with Li_2O/Li_2O GB. We would like to stress that SEI films formed from the decomposition of electrolytes are kinetically controlled self-assembled structures, not necessarily the most energetically favorable. To obtain a metastable structure, the Li interphase with each of the SEI GB structures is then systematically analyzed by manually adding Li into these structures at specific locations close to the interphase, specifically at the TPB and other open sites.

The "Interface Builder" from the Atomistic Tool Kit (ATK)[50] package is used to build the GB structures. This tool helps to analyze every possible interphase structure between two slabs. The algorithm searches every angular orientation (with 2° steps) between the two slabs to create a supercell with the least amount of strain at the interface. Since there are infinite number of GBs that could be possible, specific cutoffs such as a maximum interphase width of 2 Å and a maximum interface strain of 5% are applied. In addition, the configurations with more than 350 atoms in the supercell were not analyzed due to the computational limitation of the DFT method.

3.1.1. LiF/Li_2O GB on the Li Surface. The LiF/Li_2O GB on Li is first analyzed, as shown in Figure 2a, as it gives the rate-determining step for Li diffusion across the SEI grain structure and provides a faster diffusion pathway for Li diffusion. The interfacial arrangement of the LiF/Li_2O interphase on Li, where the Li_2O and LiF layers are placed with the oxygen and fluorine facets exposed to the Li metal, provides a stable conformational structure. From the final optimized configuration, it could be seen clearly that the topmost Li metal layer undergoes a significant amount of strain and becomes part of the LiF structure by shifting electronic charges into the LiF

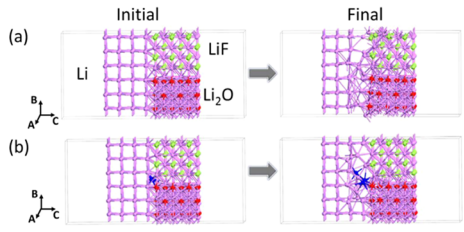

Figure 2. (a) Initial and final optimized structures of LiF/Li_2O GB on the Li surface with no added Li at the TPB, and (b) initial and final optimized structures of LiF/Li_2O GB on Li with added Li at TPB.

https://dx.doi.org/10.1021/acsaem.0c01605
ACS Appl. Energy Mater. XXXX, XXX, XXX−XXX

sublattice. The existence of GBs at the solid−solid interphases allows electron transfer to the LiF or Li_2O upon contact and significant rearrangement at the TPB and LiF/Li_2O structures, resulting in an unstable configuration.

As mentioned in the previous sections, the growth and stability of SEI are highly kinetically driven processes, and to achieve a metastable state and systematically evaluate the nucleation of dendrites, we attempt to insert Li incrementally at the TPB interfaces, starting with one Li adatom, as shown in Figure S1 (Supporting Information). On addition of Li at the TPB sites, it can be observed that the rearrangement on the LiF/Li_2O slab is minimal and the stability of the structure is improved. However, with the inclusion of more Li adatoms than the number of available sites in the TPB, the TPB starts to diverge, resulting in an unstable configuration. Since this study attempts to capture the stability of these metastable structures, the structures with unstable configurations are not shown in the current results and are not used for excess energy calculations. To visualize the reduction of rearrangement on the Li surface due to the addition of Li, the case with three added Li adatoms is shown in comparison to the case with no added Li in Figure 2b. In Figures 2−7, the pink, red, and green colored spheres depict Li, O, and F atoms, respectively. The added Li atoms are shown in blue.

To quantify the stability of the TPB structures, further analyses are required to understand and compare the stability of different SEI components on the Li metal surface, which is discussed in Section 3.1.4.

3.1.2. Li_2O/Li_2O GB on the Li Surface. For Li_2O/Li_2O GB, the structure search method using ATK, as shown in Section 2, resulting in a structure equivalent to a strained bcc Li structure for the Li slab, cleaved along its (110) plane, and has surface energy closer to the (001) Li surface, as shown in Figure 3a.

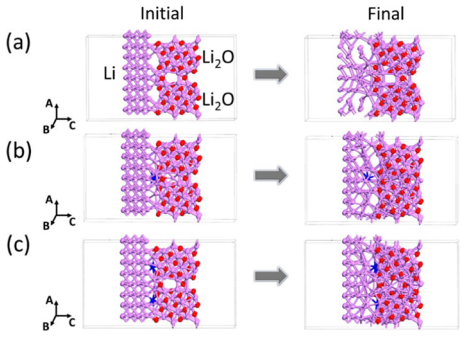

Figure 3. (a) Initial and final optimized structures of Li_2O/Li_2O GB on the Li surface with no added Li atom at the TPB, (b) initial and final optimized structures of Li_2O/Li_2O GB on Li with added Li at TPB, and (c) initial and final optimized structures of Li_2O/Li_2O GB on Li with added Li at other sites in the interphase.

Similar to LiF/Li_2O GB structures, the Li_2O/Li_2O GB on Li interphases shows a significant distortion in the first layers of Li and the Li_2O/Li_2O GB, as shown in the final configuration of Figure 3a. On further addition of Li at the TPB sites, it can be observed that a similar trend to LiF/Li_2O GB is followed and the rearrangement on the Li_2O/Li_2O GB slab is minimized, resulting in improved stability of the structure, rendering it metastable. The increment of the number of Li adatoms and its effect on the Li surface is shown in Figure S2 of the Supporting Information. Since Li_2O/Li_2O GB has fractional surfaces of Li_2O, more possible locations for Li insertion are present in these TPB structures unlike LiF/Li_2O-based TPB structures, as shown in Figure 3b,c.

3.1.3. LiF/LiF GB on the Li Surface. The initial and the final relaxed interfacial supercells of LiF/LiF GB structures on the Li metal surface are as shown in Figure 4a (initial and final). In

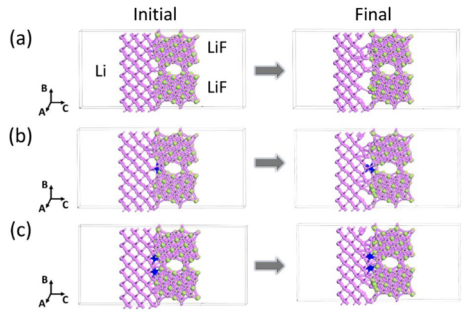

Figure 4. (a) Initial and final optimized structures of LiF/LiF GB on the Li surface with no added Li at the TPB, (b) initial and final optimized structures of LiF/LiF GB on Li with added Li at TPB, and (c) initial and final optimized structures of LiF/LiF GB on Li with added Li at other sites in the interphase.

contrast to the LiF/Li_2O GB and Li_2O/Li_2O GB, the relaxed LiF/LiF GB on Li interfaces experienced the least amount of distortion in the lattice, specifically in the interface region where only a slight bending of the atomic layer is observed. The increment of the number of Li adatoms and its effect on the Li surface is shown in Figure S3 of the Supporting Information. However, a similar trend of reduction in distortion with the SEI structures is observed when Li atoms are added near the interface at the TPB sites, as shown in Figure 4b,c.

3.1.4. Stability of SEI Grain Structures on the Li Surface. As mentioned in the previous sections, to quantitatively analyze the stability of different SEI grain structures on the Li surface and compare them against each other, the per atom binding energy (E_b) of Li in the TPB structures are calculated as computed overpotential

$$V = -\frac{[E_b - n_i E_{Li}]}{n_i |e|} \quad (1)$$

where the number of inserted Li atoms is given by n_i and the charge of an electron is denoted by $|e|$. The overpotential definition corresponds to the overpotential defined in the work of Leung et al.[31] From a physical perspective, the values of overpotentials are determined from kinetic constraints. Thus, the definition of V in this work is used as a way to describe the insertion energy more conveniently. We believe that the usage of per atom binding energy subtracted by the energy of Li, instead of the total energy per atom including the Li atoms would be a good quantitative measure for comparison since it subtracts the energy of Li and removes the effect of averaging with low-energy Li atoms. In Table 2, the energetics of all of the analyzed configurations are shown for all of the three combinations of SEI components on the Li surface.

The comparison of overpotentials due to Li's addition at these interface structures illustrates that the LiF/LiF GB is the most stable structure on the Li surface of the three, followed by Li_2O/Li_2O and finally the LiF/Li_2O grain structure on Li. This mechanical and electrochemical stability of LiF compared with Li_2O could be essential in explaining the relative morphological stability and better cycling of Li metal anodes with electrolytes

https://dx.doi.org/10.1021/acsaem.0c01605
ACS Appl. Energy Mater. XXXX, XXX, XXX−XXX

Table 2. Binding Energy-Based Overpotential for Different SEI Grain Structures on the Li Surface

chemical system			
chemical system	configuration	total energy per atom (eV/atom)	overpotential (V)
LiF/Li_2O on Li	with no added Li	−3.632	NA
	with one added Li at TPB	−3.711	−1.51
	with two added Li at TPB	−3.763	−1.49
	with three added Li at TPB	−3.772	−1.47
Li_2O/Li_2O on Li	with no added Li	−3.721	NA
	with one added Li at TPB	−3.770	−1.44
	with two added Li at TPB	−3.791	−1.42
	with two added Li at the Li/SEI interface	−3.813	−1.40
LiF/LiF on Li	with no added Li	−3.812	NA
	with one added Li at TPB	−3.880	−1.38
	with two added Li at TPB	−3.933	−1.37
	with two added Li at the Li/SEI interface	−3.951	−1.36

such as $LiPF_6$, which are known to produce LiF during SEI formation. From Table 2, it is also evident that by adding Li on to the interface at specific locations the stability of the SEI/Li interface is improved. However, on further addition of Li to these interfaces, the structure starts to form cracks along the GB region.

The reduction in the magnitude of overpotential, as shown in Table 2, suggests the improvement in the stability when Li is added to the Li/SEI interface. However, to further qualitatively examine this phenomenon, the isosurfaces of charge densities are plotted, specifically close to the interphase, and the interaction at the interphase between the SEI and the Li slabs is observed. Figure 5 shows the charge density isosurfaces of

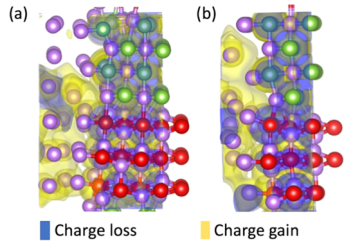

Figure 5. Charge density difference maps of LiF/Li_2O GB on the Li surface (a) with no added Li^0 and (b) with added Li at the TPB. The isosurface scale is chosen as 0.001 e/A^3.

the optimized structures shown in Figure 2. The highly electronegative fluorine and oxygen lose charge, and the Li closer to the interface moves toward the interphase and gains the charge. From the structures shown in Figure 5, we observe more interaction at the interface after adding additional adatoms to the structure. The isosurface scale is chosen to be 0.001 e/A^3 for all of the structures analyzed. In the charge density isosurface, yellow indicates regions of charge gain and blue indicates regions of charge loss.

In Figures 6a–c and 7a–c, the electron density maps of the Li_2O/Li_2O GB and LiF/LiF GB on the Li surface are shown,

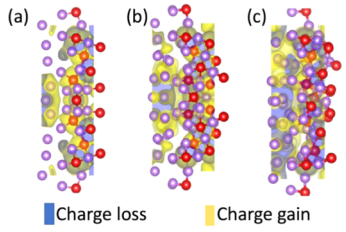

Figure 6. Charge density difference maps of Li_2O/Li_2O GB on the Li surface (a) with no added Li, (b) with added Li at the TPB, and (c) with added Li at other interfacial sites. The isosurface scale is chosen as 0.001 e/A^3.

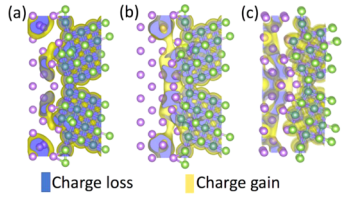

Figure 7. Charge density difference maps of LiF/LiF GB on the Li surface (a) with no added Li, (b) with added Li at other interfacial sites, and (c) with added Li at the TPB. The isosurface scale is chosen as 0.001 e/A^3.

respectively. In these structures, the addition of Li at the TPB improves the interaction and electron transfer at the interphase, making it more favorable. However, since the GB structures of SEI are made of the fractional surfaces of LiF and Li_2O, there is still lesser interaction near the top and bottom of the TPB, which is further improved by adding more Li into these sites.

3.2. Excess Energy and Stability of TPB. To evaluate the role of the SEI on the Li dendrite suppression, the favorability for dendritic growth along the TPB is evaluated based on energy analysis. When the Li dendrite grows through the GB of brittle SEI, the strain energy at the tip of the GB will be released and work is required to form the new interphase. Since the TPBs are the weakest points in SEI structures, the excess energy due to TPB is the energy required by the dendrites to nucleate through the SEI grain structures.

The most stable and naturally forming surfaces in the grain structure of SEI are generally the minimum energy surfaces. Thus, these surfaces are created and the surface energies per unit area of a slab are calculated. The surface energy, as shown in eq 2, is calculated using the total energy of the slab structure and the bulk energy of the same component as the slab with the same number of atoms

$$\gamma_{\text{surf}}^{\text{A}} = \frac{E_{\text{slab}}^{\text{A}} - N_{\text{A}} E_{\text{bulk}}}{S} \tag{2}$$

where $\gamma_{\text{surf}}^{\text{A}}$ denotes the surface energy per unit area of the slab A, $E_{\text{slab}}^{\text{A}}$ denotes the total energy of the slab, E_{bulk} is the energy per unit cell of the bulk structure of A, N denotes the number of units, and S is the surface area. The calculated surface energies for the SEI grain structures have already been reported in our previous work[16] and are used in this work to calculate the GB energies.

Similarly, the GB energy densities for all of the interphases in the TPB structure are evaluated. The GB energy density is calculated as shown in the equation3

https://dx.doi.org/10.1021/acsaem.0c01605
ACS Appl. Energy Mater. XXXX, XXX, XXX−XXX

$$\gamma_{GB} = \frac{E_{GB}^{AB} - N_A E_A - N_B E_B}{2S} \quad (3)$$

where γ_{GB} is the interfacial energy density and E_{GB}^{AB} is the total energy of the relaxed TPB structure. Also, E_A and E_B denote the total energies of structures A and B, respectively, where A and B are slabs on either side of the interphase. Table 3 lists

Table 3. Surface Orientations and GB Energies of Different SEI Components

chemical system	GB energies (meV/Å^2)	GB density (1/Å)
LiF/LiF	23.80	0.130
Li_2O/Li_2O	34.08	0.118
LiF/Li_2O	18.01	0.124

the calculated interfacial GB energy per unit area of the interphase between the SEI grain structures and the GB density, evaluated as $\rho = 2S/abc$. The calculated surface energies, as shown in Table 3, for the SEI grain structures have already been reported in our previous work[16] and are used in this work to calculate the GB energies.

The interfacial GB energies for the interphases between SEI and Li are calculated using the same relation as shown in eq 2, by assuming the SEI (LiF/LiF, Li_2O/Li_2O or LiF/Li_2O) as one slab and Li as the second slab. The GB interfacial energies for the SEI/Li interfaces are as shown in Table 3. The GB energy densities, as shown in Tables 3 and 4, suggest that LiF/LiF GB has much better stability when compared to Li_2O/Li_2O on the Li metal surface, although the Li_2O/Li_2O GB system is more stable as a GB than LiF/LiF GB.

Table 4. Surface Orientations and GB Energies of Different SEI GBs on the Li Surface

chemical system			
chemical system	Li slab surface	GB energies (meV/Å^2)	GB density (1/Å)
LiF/LiF on Li	(001)	28.34	0.161
Li_2O/Li_2O on Li	(110)	75.42	0.153
LiF/Li_2O on Li	(001)	11.65	0.148

To further enhance this understanding and address the energies specific to the TPB, the excess energy due to the formation of TPB is calculated using the cohesive energy of the pristine slabs. The excess energy of TPB and the stability of the interphases are calculated based on the cohesive energies and the GB interphase energies of the SEI components and Li metal. The excess energy due to TPB formation is calculated using the equation4

$$\gamma_{TPB} = \frac{E_{TPB} - \sum_{i=1}^{3} n_i E_{i,coh} - \sum_{i=1}^{3} \gamma_{i,GB} S_{i,GB}}{l_{TPB}} \quad (4)$$

where E_{TPB} is the total energy of the TPB structure, $E_{i,coh}$ is the cohesive energy per unit atom of each component in the TPB structure, n is the total no. of atoms in every component, $\gamma_{i,GB}$ is the grain boundary energy density along each of the GBs, $S_{i,GB}$ is the surface area of the interphase in the TPB structure, and l_{TPB} is the TPB length. The TPB length is defined as the length measured across the Li/SEI interphase along the TPB. The greater is the value of γ_{TPB}, and the higher is the stability of the SEI grain structure on Li.

On the basis of eq 4, for a given SEI grain structure, the excess energy due to TPB decreases with the increase in GB energy densities of all of the interphases that form the TPB and the cohesive energies of the SEI components. The excess energy of TPB is calculated to be −0 eV/Å for LiF/LiF GB on the Li surface, 4.08 eV/Å for Li_2O/Li_2O on the Li surface, and −7.13 eV/Å for LiF/Li_2O on the Li surface. Although, based on total energy per unit atom, as shown in Table 2, LiF/Li_2O is less stable on the Li surface than Li_2O/Li_2O, the excess energy of TPB in Li_2O/Li_2O on the Li surface makes it more susceptible for dendritic nucleation. A strain energy per unit length of 4.08 eV/Å (Li_2O/Li_2O on Li TPB) is required at the tip of the dendrite to penetrate through the TPB and crack opens the GB and form a stable dendrite.

A stronger cohesive bonding between the LiF/LiF slab and Li indicates that it is much more favorable to have LiF/LiF grain structures on the surface of Li than Li_2O/Li_2O and LiF/Li_2O. However, since there are various electrolyte reduction reactions that compete on the formation of SEI, the SEI formation and its growth are kinetically driven and are often constrained due to the presence of other grains. They can result in some less stable Li_2O/Li_2O and LiF/Li_2O forming at the Li surface.

4. SUMMARY AND CONCLUSIONS

The morphology and deposition behavior of Li in LMBs greatly depend on the SEI structure, its mechanical stability on the Li surface, and its mechanical properties to withstand the stress. To enhance the understanding of the stability of the SEI/Li interface, interfacial supercells were constructed by creating an interface between the Li metal and two of the primary inorganic SEI components, LiF and Li_2O. These interfacial structures were further analyzed and studied using DFT. Three different combinations for the GB structures are studied, and their interphases are carefully analyzed. The calculated interfacial energy and excess energy of each interphase revealed that LiF/LiF is the most stable on the Li metal surface followed by Li_2O/Li_2O, and the least stable is LiF/Li_2O GB. Since there is only a very minimal understanding of the exact structural arrangements and the atomic configuration of the SEI grain structures, the investigated GB structures on the Li surface for the stability can be too simplified compared to the structures in the cells under operating conditions. For example, the existence of defects and/or impurities in the SEI grains could also influence the cohesive energy at the interphase and thereby affecting the stability. All things considered, the relatively low computational cost of DFT with 200−300 atoms in the GB allows for more parametric analyses that can help in achieving improved strategies to prevent the dendritic growth of Li in LMBs. Thus, the results from the present work show a definite step forward toward a more robust modeling framework to help engineer better SEI.

■ ASSOCIATED CONTENT

Supporting Information

The Supporting Information is available free of charge at https://pubs.acs.org/doi/10.1021/acsaem.0c01605.

DFT results (final optimized structural configuration) to show the effect of sequential addition of Li on TPB structures; the results are shown for LiF/Li_2O, Li_2O/Li_2O, and LiF/LiF on the Li surface (PDF)

https://dx.doi.org/10.1021/acsaem.0c01605
ACS Appl. Energy Mater. XXXX, XXX, XXX−XXX

AUTHOR INFORMATION

Corresponding Author

Ajaykrishna Ramasubramanian − *Department of Mechanical and Industrial Engineering, University of Illinois at Chicago, Chicago, Illinois 60607, United States;* orcid.org/0000-0003-3005-6665; Email: aramas9@uic.edu

Authors

Vitaliy Yurkiv − *Department of Mechanical and Industrial Engineering, University of Illinois at Chicago, Chicago, Illinois 60607, United States;* orcid.org/0000-0002-3407-891X

Tara Foroozan − *Department of Mechanical and Industrial Engineering, University of Illinois at Chicago, Chicago, Illinois 60607, United States*

Marco Ragone − *Department of Mechanical and Industrial Engineering, University of Illinois at Chicago, Chicago, Illinois 60607, United States*

Reza Shahbazian-Yassar − *Department of Mechanical and Industrial Engineering, University of Illinois at Chicago, Chicago, Illinois 60607, United States;* orcid.org/0000-0002-7744-4780

Farzad Mashayek − *Department of Mechanical and Industrial Engineering, University of Illinois at Chicago, Chicago, Illinois 60607, United States;* orcid.org/0000-0003-1187-4937

Complete contact information is available at: https://pubs.acs.org/10.1021/acsaem.0c01605

Notes

The authors declare no competing financial interest.

ACKNOWLEDGMENTS

The authors acknowledge the financial support from the National Science Foundation (Award CBET-1805938). The authors acknowledge the computational support by the Advanced Cyberinfrastructure for Education and Research (ACER) group at The University of Illinois at Chicago and the Extreme Science and Engineering Discovery Environment (XSEDE), which is supported by the National Science Foundation.

REFERENCES

(1) Whittingham, M. S. Materials Challenges Facing Electrical Energy Storage. *MRS Bull.* **2008**, *33*, 411−419.

(2) Tarascon, J. M.; Armand, M. Issues and Challenges Facing Rechargeable Lithium Batteries. *Nature* **2001**, *414*, 359−367.

(3) Tikekar, M. D.; Choudhury, S.; Tu, Z.; Archer, L. A. Design Principles for Electrolytes and Interfaces for Stable Lithium-Metal Batteries. *Nat. Energy* **2016**, *1*, No. 16114.

(4) Xu, W.; Wang, J.; Ding, F.; Chen, X.; Nasybulin, E.; Zhang, Y.; Zhang, J.-G. Lithium Metal Anodes for Rechargeable Batteries. *Energy Environ. Sci.* **2014**, *7*, 513−537.

(5) Wang, L.; Zhou, Z.; Yan, X.; Hou, F.; Wen, L.; Luo, W.; Liang, J.; Dou, S. X. Engineering of Lithium-Metal Anodes towards a Safe and Stable Battery. *Energy Storage Mater.* **2018**, *14*, 22−48.

(6) Yurkiv, V.; Foroozan, T.; Ramasubramanian, A.; Shahbazian-Yassar, R.; Mashayek, F. Phase-Field Modeling of Solid Electrolyte Interface (SEI) Influence on Li Dendritic Behavior. *Electrochim. Acta* **2018**, *265*, 609−619.

(7) Yan, H. H.; Bie, Y. H.; Cui, X. Y.; Xiong, G. P.; Chen, L. A Computational Investigation of Thermal Effect on Lithium Dendrite Growth. *Energy Convers. Manag.* **2018**, *161*, 193−204.

(8) Cheng, X. B.; Zhang, R.; Zhao, C. Z.; Zhang, Q. Toward Safe Lithium Metal Anode in Rechargeable Batteries: A Review. *Chem. Rev.* **2017**, *117*, 10403−10473.

(9) Goodenough, J. B.; Kim, Y. Challenges for Rechargeable Li Batteries. *Chem. Mater.* **2010**, *22*, 587−603.

(10) Peled, E. The Electrochemical Behavior of Alkali and Alkaline Earth Metals in Nonaqueous Battery Systems—the Solid Electrolyte Interphase Model. *J. Electrochem. Soc.* **1979**, *126*, 2047−2051.

(11) Peled, E.; Menachem, C.; BarTow, D.; Melman, A. Improved Graphite Anode for Lithium-Ion Batteries Chemically Bonded Solid Electrolyte Interface and Nanochannel Formation. *J. Electrochem. Soc.* **1996**, *143*, L4−L7.

(12) Peled, E.; Golodnitsky, D.; Ardel, G. Advanced Model for Solid Electrolyte Interphase Electrodes in Liquid and Polymer Electrolytes. *J. Electrochem. Soc.* **1997**, *144*, L208−L210.

(13) Peled, E.; Golodnttsky, D.; Ardel, G.; Menachem, C.; Bar Tow, D.; Eshkenazy, V. The Role of Sei in Lithium and Lithium Ion Batteries. *MRS Proc.* **1995**, *393*, No. 209.

(14) Cheng, X.-B.; Zhang, R.; Zhao, C.-Z.; Wei, F.; Zhang, J.-G.; Zhang, Q. A Review of Solid Electrolyte Interphases on Lithium Metal Anode. *Adv. Sci.* **2016**, *3*, No. 1500213.

(15) Yan, C.; Cheng, X. B.; Zhao, C. Z.; Huang, J. Q.; Yang, S. T.; Zhang, Q. Lithium Metal Protection through In-Situ Formed Solid Electrolyte Interphase in Lithium-Sulfur Batteries: The Role of Polysulfides on Lithium Anode. *J. Power Sources* **2016**, *327*, 212−220.

(16) Ramasubramanian, A.; Yurkiv, V.; Foroozan, T.; Ragone, M.; Shahbazian-Yassar, R.; Mashayek, F. Lithium Diffusion Mechanism through Solid−Electrolyte Interphase in Rechargeable Lithium Batteries. *J. Phys. Chem. C* **2019**, *123*, 10237−10245.

(17) Steiger, J.; Kramer, D.; Mönig, R. Microscopic Observations of the Formation, Growth and Shrinkage of Lithium Moss during Electrodeposition and Dissolution. *Electrochim. Acta* **2014**, *136*, 529−536.

(18) Steiger, J.; Kramer, D.; Mönig, R. Mechanisms of Dendritic Growth Investigated by in Situ Light Microscopy during Electrodeposition and Dissolution of Lithium. *J. Power Sources* **2014**, *261*, 112−119.

(19) Shi, S.; Gao, J.; Liu, Y.; Zhao, Y.; Wu, Q.; Ju, W.; Ouyang, C.; Xiao, R. Multi-Scale Computation Methods: Their Applications in Lithium-Ion Battery Research and Development. *Chin. Phys. B* **2016**, *25*, No. 018212.

(20) Gibbs, J. W.; Mohan, K. A.; Gulsoy, E. B.; Shahani, A. J.; Xiao, X.; Bouman, C. A.; De Graef, M.; Voorhees, P. W. The Three-Dimensional Morphology of Growing Dendrites. *Sci. Rep.* **2015**, *5*, No. 11824.

(21) Qin, X.; Shao, M.; Balbuena, P. B. Elucidating Mechanisms of Li Plating on Li Anodes of Lithium-Based Batteries. *Electrochim. Acta* **2018**, *284*, 485−494.

(22) Aryanfar, A.; Brooks, D.; Merinov, B. V.; Goddard, W. A.; Colussi, A. J.; Hoffmann, M. R. Dynamics of Lithium Dendrite Growth and Inhibition: Pulse Charging Experiments and Monte Carlo Calculations. *J. Phys. Chem. Lett.* **2014**, *5*, 1721−1726.

(23) Yoon, G.; Moon, S.; Ceder, G.; Kang, K. Deposition and Stripping Behavior of Lithium Metal in Electrochemical System: Continuum Mechanics Study. *Chem. Mater.* **2018**, *30*, 6769−6776.

(24) Hong, Z.; Viswanathan, V. Phase-Field Simulations of Lithium Dendrite Growth with Open-Source Software. *ACS Energy Lett.* **2018**, *3*, 1737−1743.

(25) Liu, G.; Lu, W. A Model of Concurrent Lithium Dendrite Growth, SEI Growth, SEI Penetration and Regrowth. *J. Electrochem. Soc.* **2017**, *164*, A1826−A1833.

(26) Ozhabes, Y.; Gunceler, D.; Arias, T. A. Stability and Surface Diffusion at Lithium-Electrolyte Interphases with Connections to Dendrite Suppression. 2015, arXiv:1504.05799. arXiv.org e-Print archive. https://arxiv.org/abs/1504.05799.

(27) Ely, D. R.; García, R. E. Heterogeneous Nucleation and Growth of Lithium Electrodeposits on Negative Electrodes. *J. Electrochem. Soc.* **2013**, *160*, A662−A668.

(28) Pei, A.; Zheng, G.; Shi, F.; Li, Y.; Cui, Y. Nanoscale Nucleation and Growth of Electrodeposited Lithium Metal. *Nano Lett.* **2017**, *17*, 1132−1139.

https://dx.doi.org/10.1021/acsaem.0c01605
ACS Appl. Energy Mater. XXXX, XXX, XXX−XXX

(29) Chazalviel, J. N. Electrochemical Aspects of the Generation of Ramified Metallic Electrodeposits. *Phys. Rev. A* **1990**, *42*, 7355−7367.
(30) Christensen, J.; Newman, J. A Mathematical Model for the Lithium-Ion Negative Electrode Solid Electrolyte Interphase. *J. Electrochem. Soc.* **2004**, *151*, A1977−A1988.
(31) Leung, K.; Jungjohann, K. L. Spatial Heterogeneities and Onset of Passivation Breakdown at Lithium Anode Interfaces. *J. Phys. Chem. C* **2017**, *121*, 20188−20196.
(32) Yurkiv, V.; Foroozan, T.; Ramasubramanian, A.; Ragone, M.; Shahbazian-Yassar, R.; Mashayek, F. Understanding Zn Electrodeposits Morphology in Secondary Batteries Using Phase-Field Model. *J. Electrochem. Soc.* **2020**, *167*, No. 060503.
(33) Yurkiv, V.; Gutiérrez-Kolar, J. S.; Unocic, R. R.; Ramsubramanian, A.; Shahbazian-yassar, R.; Mashayek, F. Competitive Ion Diffusion within Grain Boundary and Grain Interiors in Polycrystalline Electrodes with the Inclusion of Stress Field. *J. Electrochem. Soc.* **2017**, *164*, A2830−A2839.
(34) Shi, S.; Qi, Y.; Li, H.; Hector, L. G. Defect Thermodynamics and Diffusion Mechanisms in Li_2CO_3 and Implications for the Solid Electrolyte Interphase in Li-Ion Batteries. *J. Phys. Chem. C* **2013**, *117*, 8579−8593.
(35) Soto, F. A.; Marzouk, A.; El-Mellouhi, F.; Balbuena, P. B. Understanding Ionic Diffusion through SEI Components for Lithium-Ion and Sodium-Ion Batteries: Insights from First-Principles Calculations. *Chem. Mater.* **2018**, *30*, 3315−3322.
(36) Edström, K.; Herstedt, M.; Abraham, D. P. A New Look at the Solid Electrolyte Interphase on Graphite Anodes in Li-Ion Batteries. *J. Power Sources* **2006**, *153*, 380−384.
(37) Lu, M.; Cheng, H.; Yang, Y. A Comparison of Solid Electrolyte Interphase (SEI) on the Artificial Graphite Anode of the Aged and Cycled Commercial Lithium Ion Cells. *Electrochim. Acta* **2008**, *53*, 3539−3546.
(38) Zhuang, G. V.; Ross, P. N. Analysis of the Chemical Composition of the Passive Film on Li-Ion Battery Anodes Using Attentuated Total Reflection Infrared Spectroscopy. *Electrochem. Solid-State Lett.* **2003**, *6*, A136−A139.
(39) Parimalam, B. S.; MacIntosh, A. D.; Kadam, R.; Lucht, B. L. Decomposition Reactions of Anode Solid Electrolyte Interphase (SEI) Components with LiPF6. *J. Phys. Chem. C* **2017**, *121*, 22733−22738.
(40) Aurbach, D.; Markovsky, B.; Rodkin, A.; Cojocaru, M.; Levi, E.; Kim, H.-J. An Analysis of Rechargeable Lithium-Ion Batteries after Prolonged Cycling. *Electrochim. Acta* **2002**, *47*, 1899−1911.
(41) Nie, M.; Chalasani, D.; Abraham, D. P.; Chen, Y.; Bose, A.; Lucht, B. L. Lithium Ion Battery Graphite Solid Electrolyte Interphase Revealed by Microscopy and Spectroscopy. *J. Phys. Chem. C* **2013**, *117*, 1257−1267.
(42) Nie, M.; Abraham, D. P.; Chen, Y.; Bose, A.; Lucht, B. L. Silicon Solid Electrolyte Interphase (SEI) of Lithium Ion Battery Characterized by Microscopy and Spectroscopy. *J. Phys. Chem. C* **2013**, *117*, 13403−13412.
(43) Kresse, G.; Furthmüller, J. Efficient Iterative Schemes for Ab Initio Total-Energy Calculations Using a Plane-Wave Basis Set. *Phys. Rev. B* **1996**, *54*, 11169−11186.
(44) Blöchl, P. E. Projector Augmented-Wave Method. *Phys. Rev. B* **1994**, *50*, 17953−17979.
(45) Perdew, J. P.; Ruzsinszky, A.; Csonka, G. I.; Vydrov, O. A.; Scuseria, G. E.; Constantin, L. A.; Zhou, X.; Burke, K. Restoring the Density-Gradient Expansion for Exchange in Solids and Surfaces. *Phys. Rev. Lett.* **2008**, *100*, No. 136406.
(46) Perdew, J. P.; Burke, K.; Ernzerhof, M. Generalized Gradient Approximation Made Simple. *Phys. Rev. Lett.* **1996**, *77*, 3865−3868.
(47) Ma, C.; Cheng, Y.; Yin, K.; Luo, J.; Sharafi, A.; Sakamoto, J.; Li, J.; More, K. L.; Dudney, N. J.; Chi, M. Interfacial Stability of Li Metal−Solid Electrolyte Elucidated via in Situ Electron Microscopy. *Nano Lett.* **2016**, *16*, 7030−7036.
(48) Leung, K.; Tenney, C. M. Toward First Principles Prediction of Voltage Dependences of Electrolyte/Electrolyte Interfacial Processes in Lithium Ion Batteries. *J. Phys. Chem. C* **2013**, *117*, 24224−24235.
(49) Leung, K. Predicting the Voltage Dependence of Interfacial Electrochemical Processes at Lithium-Intercalated Graphite Edge Planes. *Phys. Chem. Chem. Phys.* **2015**, *17*, 1637−1643.
(50) Atomistix Toolkit *Synopsys QuantumWise*. version 2016.4

https://dx.doi.org/10.1021/acsaem.0c01605
ACS Appl. Energy Mater. XXXX, XXX, XXX−XXX